Pedestal modes Interactions Triggering Bursts and Leading to the onset of Edge Localized Modes on DIII-D

A. Diallo[1], J. Dominski[1], K. Barada[2], F. Laggner[1], M. Knolker[3], G.J. Kramer[1], T.L. Rhodes[2], L. Zeng[2], and G. McKee[4]

[1] *Princeton Plasma Physics Laboratory, P.O. 451, Princeton, NJ, USA*

[2] *Physics Department, University of California Los Angeles, Los Angeles, CA, USA*

[3] *General Atomics, San Diego, CA, USA*

[4] *University of Wisconsin-Madison, 1500 Engineering Dr., Madison, WI, USA*

During an edge localized mode (ELM) event, the plasma suddenly erupts releasing a significant fraction of its stored energy over few microseconds. The working hypothesis for the onset of ELM is the destabilization of magnetohydrodynamic instabilities, namely ideal peeling-ballooning modes[1;2]. A body of literature[1;3;4] supports the paradigm of coupled peeling ballooning (PB) modes as the *driver* of ELM events. Refs.[5;6] have alternatively pointed out that ELMs are the result of a basic detonation scenario, where a ballooning instability nonlinearly grows explosively. While the PB theory and the explosive scenario have appealing features that could explain ELMs, the ELM onset mechanism remains elusive – specifically when the edge parameters can exist near the stability margin for a substantial part of the period preceding the ELM onset. Here, we discuss experimental results indicating that pedestal mode nonlinear

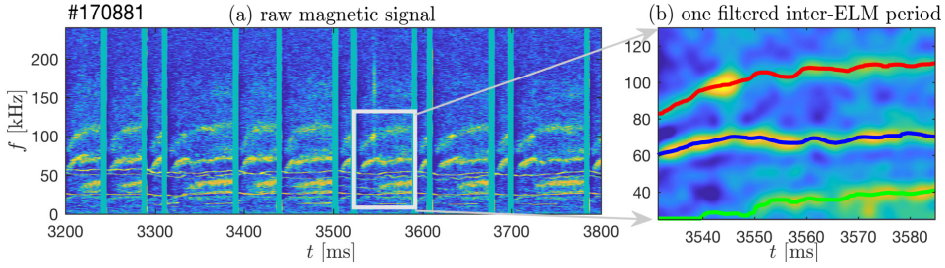

Figure 1: Example spectrogram of the magnetic fluctuations for shot 170881. (a) Magnetic spectrogram during multiple ELMs. Here the ELMs are represented by the thick vertical lines. Typical rise time of these ELMs is $\simeq 80\mu s$. (b) Zoomed spectrogram over a shorter time window where the core modes have been filtered out.

interactions can lead up to either bursts or ELM onset. Our previous work (Diallo et al. EPS 2018) suggests that the bursts are caused by sudden nonlinear coupling with saturated dominant inter-ELM modes. We also speculated that these bursts appear to be reminiscent of an "aborted" ELM given that the pedestal was near the stability boundary. Basically, it is plausible that the radial extend of the nonlinear mode coupling was not sufficient to expel significant energy to resemble an ELM.

Here, we focus on pedestal mode nonlinear interactions leading to an ELM. In summary, we identified regimes where the PB provides a soft limit for the pedestal and a nonlinear mechanism

leads to the ELM onset (this work is reported in Ref.[7]).

The results leverage the many experimental results presented in Refs.[8;9;10;11;12;13], in which the fixed pedestal gradients appear to be pinned to the linear marginally stable peeling ballooning profiles prior to the ELM onset – to investigate the dynamics of the pedestal modes leading up to the onset of an ELM. Note that a summary of the pedestal turbulence has been reported in Ref.[14].

Specifically, recent experiments have shown that the pedestal density and temperature gradients after an ELM reach a quasi-stationary state[9;10;11;12] during which the pedestal structure (width and height) either evolves slowly or remains quasi-stationary for few milliseconds prior to the ELM onset. During this quasi-stationary phase between ELMs, pedestal localized modes have been observed to grow and saturate (e.g., see Refs[8;9;10;15;12;16]). These modes were observed to be correlated with the evolution of the edge profile gradients later in the ELM cycle in multiple devices, namely AUG[10;11], C-Mod[9], DIII-D[12], and JET[8].

The EPED model predicts the pedestal structure (width and height) as the intersection of local kinetic ballooning and global peeling ballooning criteria near the stability threshold at which the ELM is triggered[17]. Nonetheless, it has been observed in many experiments that the pedestal gradients are nearly stationary for last few milliseconds of ELM cycle. The question that arises is – given that the pedestal can remain locked in this state – which mechanism leads to the onset of the ELM.

The mechanism leading to the onset of an ELM event is studied on the DIII-D tokamak. The discharge is a lower-single null plasma, with plasma current of 1 MA, $\beta_n \sim 1.4$, a stored energy of 0.43 MJ, and line-averaged density of $5{\times}10^{19}$ m^{-3}. We focus on type I ELMy discharges with low ELM frequency ~20 - 30 Hz to capture the evolution of the pedestal parameters as well as the fluctuations leading up to ELMs. PB calculations during the last phase of an ELM cycle, indicate that the edge pressure gradient and current are near the stability point 4 ms prior to the ELM onset (see similar observations in refs. AUG[10;11;18], C-Mod[9], DIII-D[12], and JET[8], and discussions by Kirk *et al.* in [13]). The question that arises – why is the pedestal not erupting?

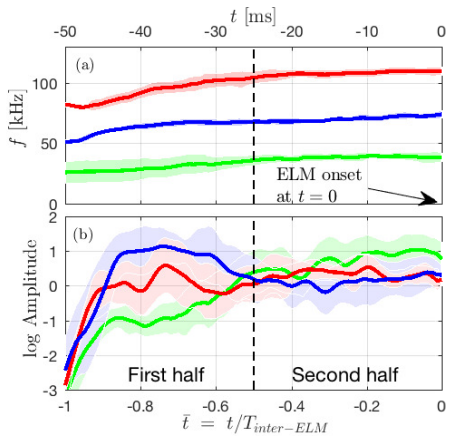

Figure 2: Dynamics of the frequency and amplitude of the three dominant modes observed in magnetic fluctuations as a function of ELM cycle [the time relative to an ELM in ms is on the top horizontal axis for reference]. The reference $t = 0$ is located at the ELM onset. (b) Associated mode amplitude evolution during the ELM cycle, in log-scale. These quantities have been statistically averaged over multiple inter-ELM periods. The shaded area represents the standard deviations.

The main diagnostics used in this analysis are the fast magnetic probes measuring fluctua-

tions in the poloidal magnetic field (referred to as $\dot{B}_\theta$) and *the spatially resolved* beam-emission spectroscopy (BES) diagnostic probing the local density fluctuations[19] (referred to as δn_e). Figure 1(a) displays the magnetic spectrograms showing quasi-coherent fluctuations between ELMs. This figure shows multiple modes between ELMs. Fig. 1(b) represents a zoomed in version of the spectrogram identifying the three dominant modes (Note each mode's amplitude and frequency were tracked between ELMs and core modes were excluded – modes whose amplitudes are not affected by the ELMs are identified as core modes.)

We systematically track their amplitude and frequency following local maxima of the spectrogram up to the ELM event. *The same color code for the three modes is used throughout the paper*. Figure 2(a) displays these mode frequencies as a function of ELM cycle $\bar{t}$, where $\bar{t} = t/T_{inter-ELM}$ and $T_{inter-ELM}$ is the normalized duration of each inter-ELM period [$\bar{t} = 0$ corresponds to the ELM onset.] Similarly, Fig. 2(b) shows the associated amplitude evolution.

To confirm that the modes, associated with frequencies above, are localized in the pedestal, we utilize the 2D BES system as shown in fig. 3(a). Figs. 3(b) and (c) display the spectrogram and power spectra, both showing the same frequencies as those observed in the magnetic signals. Figs. 3(d) and (e) show the 2D correlation map, and the dispersion relation, respectively. To further characterize the radial profiles of these three modes and their evolution during the first and second half of the ELM cycles, we analyze the correlation between the magnetic fluctuations $\dot{B}_\theta$ and the density fluctuations δn_e. We compute the correlation $\langle \dot{B}_\theta, \delta n_e \rangle$ to provide the radial profile of each of the three dominant modes. Figure 3(a) displays the BES probes. Figs. 3(b) and (c) represent the spectrogram and time-averaged spectra. Figure 3(d) displays the 2D correlation map computed using the BES probes. We then focus on the poloidal correlation lengths for each dominant mode to construct the dispersion relation (as shown in Fig. 3(e)). The three dominant modes' contributions to $\langle \dot{B}_\theta, \delta n_e \rangle$ indicate a transition from a dominant contribution of the blue mode during the first half of the ELM cycle (see Fig. 4(b)) towards a more balanced contribution between the three modes during the second half (see Fig. 4(c)). From the first half to the second one, the blue mode shows a loss in correlation $\langle \dot{B}_\theta, \delta n_e \rangle$ while the green and red modes display an increase in correlation. Figure 4(d) represents the combined radial profiles due to the three modes. The profile of the last part of the ELM cycle is clearly

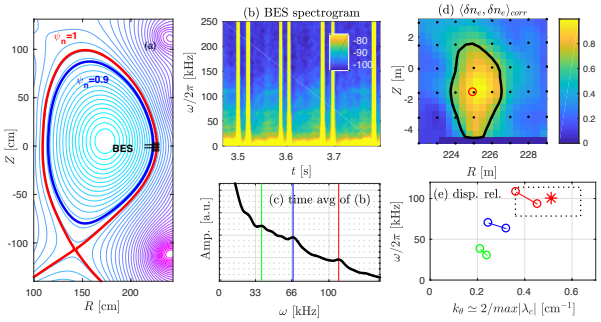

Figure 3: (a) 2D cross section with the BES probes. (b) BES spectrogram at one probes. The vertical lines indicate the ELMs. We focus on the long inter-ELM periods. (c) Time-averaged of the spectrogram to clearly show similarity between magnetic probes and BES probes spectra. (d) 2D correlation map. (e) Dispersion relation.

shifted towards the separatrix. This shift is due to the contribution of the red mode that peaks near the $q = 6$ surface (see Fig. 4(c)), in contrast to the blue and green modes which peak near $q = 5$. Given that this correlation provides a proxy for the location of the modes, Fig. 4(d) shows an outwards shift of location of the fluctuations.

In addition, Figure 4(c) and (d) suggest that there is a strong coupling between density and magnetic field near q = 6 surface. Moreover, the radial shift is consistent with Ref.[20] that suggested that there is a growth in a narrow region (e.g. pedestal) of erupting fingers pushing into the metastable region leading to the process called detonation: ELM event. Such a scenario is consistent with the nonlinear theory suggested by Ref.[6;21] in which it is shown that explosive onset of events can be attributed to the nonlinearity of MHD ballooning modes. As such, controlling the mode coupling between pedestal modes could be envisioned as another possible tool for ELM suppression.

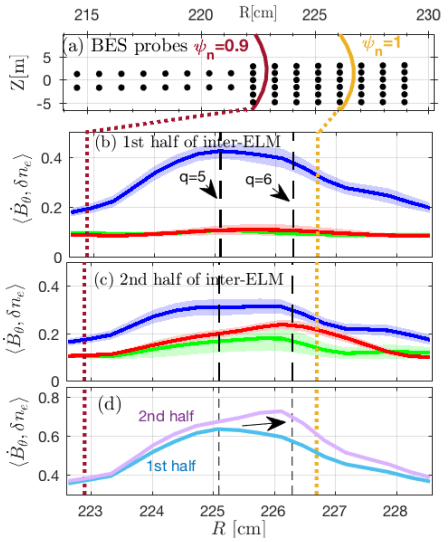

Figure 4: Radial profiles during the ELM cycle. (a) 2D map of the BES locations for reference spanning the whole pedestal $\psi_n = 0.9 - 1$. (b) Frequency resolved radial profiles of the three dominant modes using correlation between magnetic probe ($\dot{B}_\theta$) and BES chords (δn_e) during the first half of the ELM cycle and (c) during the second half of the ELM cycle. (d) Radial profiles averaged over the three dominant modes during both phases of the ELM cycle.

This material is based upon work supported by the U.S. Department of Energy, Office of Science, Office of Fusion Energy Sciences, using the DIII-D National Fusion Facility, a DOE Office of Science user facility, under Awards DE-FC02-04ER54698 No.DE-FC02-04ER54698, DE-AC02-09CH11466, DE-FG02-08ER54999, and DE-FG02-08ER54984.

References

[1] J W Connor. *Plasma Physics and Controlled Fusion*, 40(5):531, 1998;
[2] P. B. Snyder, *et al. Phys. of Plasmas*, 9:2037, 2002.
[3] H Zohm. *Plasma Phys. Control. Fusion*, 38:105, 1996.
[4] A. W. Leonard. *Physics of Plasmas (1994-present)*, 21(9):–, 2014.
[5] Steven C Cowley, *et al. Plasma Physics and Controlled Fusion*, 45(12A):A31, 2003.
[6] H. R. Wilson and S. C. Cowley. *Phys. Rev. Lett.*, 92:175006, Apr 2004.
[7] A. Diallo, *et al. Phys. Rev. Lett.*, 121:235001, Dec 2018.
[8] C P Perez, *et al. Plasma Physics and Controlled Fusion*, 46(1):61, 2004.
[9] A. Diallo, *et al. Phys. Rev. Lett.*, 112:115001, Mar 2014.
[10] F M Laggner, *et al. Plasma Physics and Controlled Fusion*, 58(6):065005, 2016.
[11] A Burckhart,*et al. Nucl. Fusion*, 52:105010, 2010.
[12] A. Diallo, *et al. Physics of Plasmas (1994-present)*, 22(5):–, 2015.
[13] A. Kirk, *et al. Nuclear Fusion*, 54(11):114012, 2014.
[14] F.M. Laggner, *et al. Nuclear Materials and Energy*, 19:479 – 486, 2019.
[15] A. Diallo, *et al. Nuclear Fusion*, 55(5):053003, 2015.
[16] X. Gao, *et al. Nuclear Fusion*, 55(8):083015, 2015.
[17] P. B. Snyder,*et al. PHYSICS OF PLASMAS*, 16(056118), 2009.
[18] J.E. Boom, *et al. Nuclear Fusion*, 52(11):114004, 2012.
[19] G. McKee, *et al. Review of Scientific Instruments*, 70(1):913–916, 1999.
[20] S. C. Cowley, *et al. Proceedings of the Royal Society of London A: Mathematical, Physical and Engineering Sciences*, 471(2180), 2015
[21] P. B. Snyder, H. R. Wilson, and X. Q. Xu. *Physics of Plasmas*, 12(5):056115, 2005.